Available online at www.sciencedirect.com

SCIENCE DIRECT®

Coastal Engineering 52 (2005) 513–533

Coastal Engineering
An International Journal for Coastal, Harbour and Offshore Engineers

www.elsevier.com/locate/coastaleng

A numerical model for wave propagation in curvilinear coordinates

Hongsheng Zhang[a,*], Liangsheng Zhu[b], Yunxiang You[a]

[a]School of Naval Architecture, Ocean and Civil Engineering, Shanghai Jiaotong University, 1954 Huashan Road, Shanghai 200030, PR China
[b]LED, South China Sea Institute of Oceanology, Chinese Academy of Sciences, 164 West Xingang Road, Guangzhou 510301, PR China

Received 24 May 2004; received in revised form 27 January 2005; accepted 10 February 2005

Abstract

Using the perturbation method, a time dependent parabolic equation is developed based on the elliptic mild slope equation with dissipation term. With the time dependent parabolic equation employed as the governing equation, a numerical model for wave propagation including dissipation term in water of slowly varying topography is presented in curvilinear coordinates. In the model, the self-adaptive grid generation method is employed to generate a boundary-fitted and varying spacing mesh. The numerical tests show that the effects of dissipation term should be taken into account if the distance of wave propagation is large, and that the outgoing boundary conditions can be treated more effectively by introduction of the dissipation term into the numerical model. The numerical model is able to give good results of simulating wave propagation for waters of complicatedly boundaries and effectively predict physical processes of wave propagation. Moreover, the errors of the analytical solution deduced by Kirby et al. (1994) [Kirby, J.T., Dalrymple, R.A., Kabu, H., 1994. Parabolic approximation for water waves in conformal coordinate systems. Coastal Engineering 23, 185–213.] from the small-angle parabolic approximation of the mild-slope equation for the case of waves between diverging breakwaters in a polar coordinate system are corrected.

Keywords: Wave propagation; Numerical model; Curvilinear coordinates; Dissipation term; Analytical solution

1. Introduction

The mild slope equation was derived by Berkhoff (1972), Smith and Sprinks (1975), Hong (1996) and other researchers in different ways. Using linear wave theory and variational principle separately, Hong (1996) proposed a mathematical model with dissipation term for combined refraction–diffraction of regular and irregular waves on non-uniform current. The above model reduces to the original mild slope equation in the current-free case without considering the dissipation term. The mild slope equation is an inseparable elliptic partial differential equation, and the solution makes prohibitive demands on computer memory and time(Panchang et al., 1991). The direct methods of solving the mild slope equation are only

* Corresponding author. Fax: +86 21 62933160/+86 21 62932147.
E-mail address: hhszhang2@sina.com.cn, hhszhang@sjtu.edu.cn (H.S. Zhang).

0378-3839/$ - see front matter © 2005 Elsevier B.V. All rights reserved.
doi:10.1016/j.coastaleng.2005.02.004

feasible when the area to be considered is small (Berkhoff et al., 1982; Li, 1994). For convenient applications, many researchers (e.g., Radder, 1979; Copeland, 1985; Li and Anastasiou, 1992; Panchang et al., 1988, 1991; Li, 1994) resorted to approximate methods of solving the mild-slope equation. These approximate methods have different characteristics respectively (Panchang et al., 1991). Using the perturbation method, Li (1994) transformed the original mild slope equation into an evolution equation, which is of time dependent parabolic type. The ADI method is used to solve the evolution equation, and the numerical scheme is unconditionally stable.

Most of the numerical models of wave propagation based on the mild slope equation are solved by the finite difference method in Cartesian coordinates. To adapt to the variable boundaries existing in coastal areas, Liu and Bolssevain (1988) and Kirby (1988) developed mathematical models based on different parabolic equations in non-orthogonal coordinate systems. Hong et al. (1999) also developed a mathematical model based on the hyperbolic equations in the same coordinate systems. But the non orthogonal coordinate systems are only fit to idealized situations involving boundary configurations (Kirby et al., 1994). Kirby et al. (1994) introduced a general formulation of small and large angle parabolic approximations in conformally mapped coordinate systems, and applied the general formulation to the study of wave propagation for two particular cases that are diverging breakwaters and circular channel. Kirby et al. (1994) also derived the exact expressions based on the original mild slope equation in a polar coordinate system for the above two cases.

Brackbill and Saltzman (1982) introduced a self adaptive grid generation method, which optimizes simultaneously grid smoothness, orthogonality and variation in volumes. The main idea is that minimizing the functions by which the three properties are measured results in a set of Euler equations, which are satisfied by the coordinate values of grid points of a mapping $x(\xi,\eta)$ or $y(\xi,\eta)$ (Liu and Zeng, 1994; Shi et al., 1997). The self adaptive grid generation method, which is not limited to a specific coordinate transformation, overcomes the drawback of an algebraic coordinate transformation. This method is widely used in numerical modeling of oceanographic problems (e.g., Shi and Sun, 1995; Shi et al., 1997). In curvilinear coordinates, Shi et al. (2001) introduced a numerical model using the Boussinesq type equations as the governing equations.

In Section 2, the elliptic mild slope equation including the dissipation term is transformed into a time dependent parabolic equation through the perturbation method. In Section 3, a numerical model is presented in curvilinear coordinates adopting the self adaptive grid generation method, and the Alternating Direction Implicit (ADI) method is employed to solve the formulated time dependent parabolic equation. In Section 4, how to deal with the boundary conditions is introduced. In Section 5, the numerical model is applied to five cases. The first case examines both the adaptability of the numerical model to oblique incidence and the effects of the dissipation term on wave propagation. The second case verifies the application for waves between diverging breakwaters with constant water depth. The third case is simulation of the waves in a circular channel. The forth case is simulation of the waves between breakwaters with varying depth for the case of oblique incidence. The fifth case is simulation of the wave propagation in the waters with complicated boundaries.

Discussing the second case, the authors improve the calculation results of the exact solution introduced by Kirby et al. (1994) (abbreviated to KDK in what follows) based on the original mild slope equation in a polar coordinate system and correct the errors of the analytical solution that KDK deduced from the small angle parabolic approximation of the mild slope equation. The waves are numerically simulated for the cases of normal and oblique incidence respectively. For the second and third cases, the effects of the dissipation term on the treating of open boundary are analyzed in detail, the present numerical model and other mathematical models are compared to the exact solution.

2. A time dependent parabolic equation with dissipation term

Using the linear wave theory and variation principle separately, Hong (1996) derived a mathematical model with dissipation term for combined refraction–diffraction waves on non-uniform current in water of slowly varying topography. The model with dissipation term in the current-free case is summarized as:

$$\frac{\partial}{\partial t}\left(\frac{\partial}{\partial t}+W^*\right)\phi-\nabla\left(\tilde{c}\tilde{c}_g\nabla\phi\right)+\left(\tilde{\sigma}^2-k^2\tilde{c}\tilde{c}_g\right)\phi=0 \tag{1}$$

wave potential

$$\varphi(x,y,z,t)=\phi(x,y,t)\frac{\cosh[k(h+z)]}{\cosh(kh)} \tag{2}$$

absolute frequency

$$\omega^2=\tilde{\sigma}^2-\frac{1}{4}W^{*2} \quad \tilde{\sigma}^2=gk\tanh(kh) \tag{3}$$

where $\phi(x,y,t)$ is complex amplitude; $\tilde{c}=((\tilde{\sigma})/(k))$; $\tilde{c}_g=((\partial\tilde{\sigma})/(\partial k))$; $h(x,y)$ is the water depth; W^* is the dissipation term and equals $\frac{4f_wH}{3\pi g}\left(\frac{K\omega}{k\sinh(kh)}\right)^3$, in which f_w is the bottom dissipation coefficient, H is the wave height, $K=\frac{Re\phi\nabla(Im\phi)-Im\phi\nabla(Re\phi)}{|\phi|^2}$. A derivation of the mathematical model with dissipation term for combined refraction–diffraction waves in the current-free case can be seen in Appendix A.

Considering the variation of wave amplitude being slowly, we introduce the slow coordinate for the time variable $\bar{t}=\varepsilon t$, where ε is a perturbation coefficient and is much smaller than unit (Li, 1994). Substituting $\phi(x,y,t)=\Psi(x,y,\bar{t})e^{-i\omega t}$ into Eq. (1) and neglecting the second order small term, we obtain a time dependent parabolic equation:

$$(-2i\omega+W^*)\frac{\partial\Psi}{\partial t}=\nabla\left(\tilde{c}\tilde{c}_g\nabla\Psi\right)-\left(\tilde{\sigma}^2-k^2\tilde{c}\tilde{c}_g\right)\Psi+\omega^2\Psi+i\omega W^*\Psi \tag{4}$$

The steady-state solution of Eq. (4) is the exact solution of the stationary mild slope equation with dissipation term for monochromatic waves. For simplicity, Eq. (4) is rewritten as:

$$f_1\frac{\partial\Psi}{\partial t}=f_2\frac{\partial\Psi}{\partial x}+f_3\frac{\partial\Psi}{\partial y}+f_4\left(\frac{\partial^2\Psi}{\partial x^2}+\frac{\partial^2\Psi}{\partial y^2}\right)+f_5\Psi \tag{5}$$

where $f_1=-2i\omega+W^*$, $f_2=((\partial(\tilde{c}\tilde{c}_g))/(\partial x))$, $f_3=((\partial(\tilde{c}\tilde{c}_g))/(\partial y))$, $f_4=\tilde{c}\tilde{c}_g$, $f_5=\omega^2-(\tilde{\sigma}^2-k^2\tilde{c}\tilde{c}_g)+i\omega W^*$.

3. Numerical scheme in curvilinear coordinates

A coordinate transformation is introduced in the general form:

$$\xi=\xi(x,y), \quad \eta=\eta(x,y) \tag{6}$$

where (ξ,η) are new independent variables in the transformed image domain. Referring to Fig. 1, the chosen boundaries Γ_1, Γ_2, Γ_3 and Γ_4 in the physical domain (x,y) thus become Π_1, Π_2, Π_3 and Π_4 respectively in the image domain (ξ,η). For further detail, the references (e.g., Brackbill and Saltzman, 1982; Liu and Zeng, 1994; Shi et al., 1997) can be referred. The ADI method is used to solve Eq. (5). Using the follow relations (f is defined as a certain function):

$$f_x=\frac{y_\eta f_\xi-y_\xi f_\eta}{J}, \tag{7}$$

$$f_y=\frac{x_\xi f_\eta-x_\eta f_\xi}{J}, \tag{8}$$

$$\begin{aligned}f_{xx}=&\left(y_\eta^2f_{\xi\xi}-2y_\xi y_\eta f_{\xi\eta}+y_\xi^2f_{\eta\eta}\right)/J^2\\&+\Big[\left(y_\eta^2y_{\xi\xi}-2y_\xi y_\eta y_{\xi\eta}+y_\xi^2y_{\eta\eta}\right)\left(x_\eta f_\xi-x_\xi f_\eta\right)\\&+\left(y_\eta^2x_{\xi\xi}-2y_\xi y_\eta x_{\xi\eta}+y_\xi^2x_{\eta\eta}\right)\left(y_\xi f_\eta-y_\eta f_\xi\right)\Big]/J^3\end{aligned} \tag{9}$$

$$\begin{aligned}f_{yy}=&\left(x_\eta^2f_{\xi\xi}-2x_\xi x_\eta f_{\xi\eta}+x_\xi^2f_{\eta\eta}\right)/J^2\\&+\Big[\left(x_\eta^2y_{\xi\xi}-2x_\xi x_\eta y_{\xi\eta}+x_\xi^2y_{\eta\eta}\right)\left(x_\eta f_\xi-x_\xi f_\eta\right)\\&+\left(x_\eta^2x_{\xi\xi}-2x_\xi x_\eta x_{\xi\eta}+x_\xi^2x_{\eta\eta}\right)\left(y_\xi f_\eta-y_\eta f_\xi\right)\Big]/J^3\end{aligned} \tag{10}$$

$$\begin{aligned}f_{xy}=&\left[\left(x_\xi y_\eta+x_\eta y_\xi\right)f_{\xi\eta}-x_\xi y_\xi f_{\eta\eta}-x_\eta y_\eta f_{\xi\xi}\right]/J^2\\&+\left[\left(x_\xi y_{\eta\eta}-x_\eta y_{\xi\eta}\right)/J^2+\left(x_\eta y_\eta J_\xi-x_\xi y_\eta J_\eta\right)/J^3\right]f_\xi\\&+\left[\left(x_\eta y_{\xi\xi}-x_\xi y_{\xi\eta}\right)/J^2+\left(x_\xi y_\xi J_\eta-x_\eta y_\xi J_\xi\right)/J^3\right]f_\eta\end{aligned} \tag{11}$$

where

$$J=x_\xi y_\eta-x_\eta y_\xi. \tag{12}$$

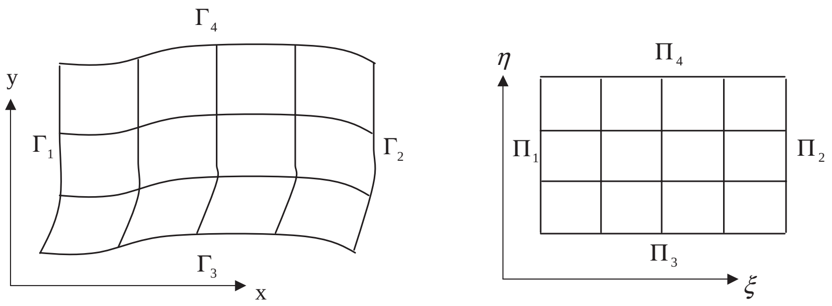

Fig. 1. Physical domain (x,y) and transformed image domain (ξ,η).

The numerical scheme of the ADI for governing Eq. (5) in curvilinear coordinates is:

$$f_1 \frac{\Psi_{i,j}^{n+1/2} - \Psi_{i,j}^{n}}{\frac{1}{2}\Delta t} = E_1\left(\frac{\partial \Psi}{\partial \xi}\right)_{i,j}^{n+1/2} + E_2\left(\frac{\partial \Psi}{\partial \eta}\right)_{i,j}^{n} + G_1\left(\frac{\partial^2 \Psi}{\partial \xi^2}\right)_{i,j}^{n+1/2} + G_2\left(\frac{\partial^2 \Psi}{\partial \eta^2}\right)_{i,j}^{n} + G_3\left(\frac{\partial^2 \Psi}{\partial \xi \partial \eta}\right)_{i,j}^{n} + \frac{f_5}{2}\left(\Psi_{i,j}^{n+1/2} + \Psi_{i,j}^{n}\right) \tag{13}$$

$$f_1 \frac{\tilde{\Psi}_{i,j}^{n+1} - \Psi_{i,j}^{n+1/2}}{\frac{1}{2}\Delta t} = E_1\left(\frac{\partial \Psi}{\partial \xi}\right)_{i,j}^{n+1/2} + E_2\left(\frac{\partial \tilde{\Psi}}{\partial \eta}\right)_{i,j}^{n+1} + G_1\left(\frac{\partial^2 \Psi}{\partial \xi^2}\right)_{i,j}^{n+1/2} + G_2\left(\frac{\partial^2 \tilde{\Psi}}{\partial \eta^2}\right)_{i,j}^{n+1} + G_3\left(\frac{\partial^2 \Psi}{\partial \xi \partial \eta}\right)_{i,j}^{n+1/2} + \frac{f_5}{2}\left(\tilde{\Psi}_{i,j}^{n+1} + \Psi_{i,j}^{n+1/2}\right) \tag{14}$$

where

$$E_1 = f_2 \frac{y_\eta}{J} - f_3 \frac{x_\eta}{J} + f_4\left(x_\eta A_1 - y_\eta A_2\right) + f_4\left(x_\eta B_1 - y_\eta B_2\right) \tag{15}$$

$$E_2 = -f_2 \frac{y_\xi}{J} + f_3 \frac{x_\xi}{J} + f_4\left(y_\xi A_2 - x_\xi A_1\right) + f_4\left(y_\xi B_2 - x_\xi B_1\right) \tag{16}$$

$$G_1 = f_4\left(\frac{y_\eta^2 + x_\eta^2}{J^2}\right) \tag{17}$$

$$G_2 = f_4\left(\frac{y_\xi^2 + x_\xi^2}{J^2}\right) \tag{18}$$

$$G_3 = -2\left(\frac{f_4 y_\xi y_\eta + f_5 x_\xi x_\eta}{J^2}\right) \tag{19}$$

$$A_1 = \left(y_\eta^2 y_{\xi\xi} - 2y_\xi y_\eta y_{\xi\eta} + y_\xi^2 y_{\eta\eta}\right)/J^3 \tag{20}$$

$$A_2 = \left(y_\eta^2 x_{\xi\xi} - 2y_\xi y_\eta x_{\xi\eta} + y_\xi^2 x_{\eta\eta}\right)/J^3 \tag{21}$$

$$B_1 = \left(x_\eta^2 y_{\xi\xi} - 2x_\xi x_\eta y_{\xi\eta} + x_\xi^2 y_{\eta\eta}\right)/J^3 \tag{22}$$

$$B_2 = \left(x_\eta^2 x_{\xi\xi} - 2x_\xi x_\eta x_{\xi\eta} + x_\xi^2 x_{\eta\eta}\right)/J^3. \tag{23}$$

To improve the convergence rate, a relaxation factor λ is introduced (Pan et al., 2000):

$$\Psi_{i,j}^{n+1} = \lambda \tilde{\Psi}_{i,j}^{n+1} + (1-\lambda)\Psi_{i,j}^{n} \tag{24}$$

where $0<\lambda\leq 1$. The time variable in the model is only an iterative parameter without any physical meanings and it would only affect the convergent speed. How to chose Δt can be referred in Li (1994).

Eqs. (13) and (14) generate tridiagonal algebraic systems and can be solved by the Gauss elimination method very efficiently. Firstly the proper initial condition is given, then iteration in the time domain is carried out until the steady-state solution is obtained. The convergence criterion is determined by the residual δ as follows

$$\delta = \frac{\sqrt{\sum_{i,j} |\Psi^n_{i,j} - \Psi^{n-1}_{i,j}|^2}}{\sum_{i,j} |\Psi^n_{i,j}|} \tag{25}$$

The program should be stopped when δ is less than 0.00003.

4. Boundary conditions

Although Eq. (4) is time dependent in form, only its steady-state solution is what is needed. The initial condition can be set as zero. Therefore the governing equation is essentially a boundary value problem with the same boundary conditions as those for the elliptic mild-slope equation.

4.1. Incident boundary conditions

If the effect of reflected waves is negligible at the incident boundary, the boundary condition can be expressed as

$$\Psi_0 = -\frac{igH_0}{2\omega} e^{i(kx\cos\theta_0 + ky\sin\theta_0)} \tag{26}$$

where Ψ_0, H_0 and θ_0 are the complex amplitude, wave height and wave direction respectively at the initial boundary.

4.2. General boundary conditions

Hong et al. (1998) and Zhang (2000) introduced general boundary conditions including open and fixed boundary conditions with arbitrary reflective properties. The general boundary conditions can effectively reflect the influence of different boundaries, and can be utilized easily. The expression suitable to the present numerical model is

$$\frac{\partial \Psi}{\partial n} + B\Psi = 0 \tag{27}$$

where

$$B = B_R + iB_I = iK\sin(\theta - \gamma)\frac{1-R}{1+R} \tag{28}$$

$$B_R = K\sin(\theta - \gamma)\frac{2R_r \sin\varepsilon_r}{1 + R_r^2 + 2R_r\cos\varepsilon_r} \tag{29}$$

$$B_I = K\sin(\theta - \gamma)\frac{1 - R_r^2}{1 + R_r^2 + 2R_r\cos\varepsilon_r} \tag{30}$$

in which θ is the wave angle at boundary, namely, the angle included between wave ray and x-axis; γ is the angle of the tangent line on the interface, namely, the angle included between the tangent line and x-axis; R is complex reflection coefficient and $R = R_r e^{i\varepsilon_r}$, where R_r and ε_r represent reflection coefficient and phase difference respectively.

If the boundary is a fully reflection one, R_r should equal to unit. Therefore Eq. (27) can be simplified as

$$\frac{\partial \Psi}{\partial n} = 0. \tag{31}$$

If the boundary is an open one, R_r should equal to zero. Therefore Eq. (27) can be simplified as

$$\frac{\partial \Psi}{\partial n} + iK\sin(\theta - \gamma)\Psi = 0. \tag{32}$$

However the main difficulty in the application of Eq. (32) is that the wave angles at the outgoing boundary are usually unknown and should be determined by iteration. An approach called boundary dissipation method (Zhang et al., 2003) is used to deal with the open boundary. There are no waves transmitting into the calculation domain through the open boundary so that the wave values outside the boundary have no effect on the wave field inside. The bottom dissipation coefficient on 3 to 5 lines of grids can be set large enough to dissipate the waves to very small near the outgoing boundary, or, if the "exact" values on the boundary are needed, one may add 3 to 5 lines of grids outside the open boundary and set the bottom dissipation coefficient large enough.

4.3. Numerical scheme of the lateral boundary conditions

In Cartesian coordinates, the normal partial differential at the left boundary (Look towards the direction of incident wave) is expressed as

$$\frac{\partial}{\partial n_1} = -\sin\gamma_1 \frac{\partial}{\partial x} + \cos\gamma_1 \frac{\partial}{\partial y} \tag{33}$$

where γ_1 is the angle included between tangent line at the left boundary and x-axis.

The normal partial differential at the right boundary is expressed as

$$\frac{\partial}{\partial n_2} = \sin\gamma_2 \frac{\partial}{\partial x} - \cos\gamma_2 \frac{\partial}{\partial y} \tag{34}$$

where γ_2 is the angle included between tangent line at the right boundary and x-axis.

In curvilinear coordinates, the normal partial differential at the left boundary is expressed as (Zhang, 2002)

$$-\frac{\partial \Psi}{\partial \zeta}\left[\frac{y_\eta \sin\gamma_1 + x_\eta \cos\gamma_1}{J}\right] + \frac{\partial \Psi}{\partial \eta}\left[\frac{y_\zeta \sin\gamma_1 + x_\zeta \cos\gamma_1}{J}\right] + B\Psi = 0 \tag{35}$$

the normal partial differential at the right boundary is expressed as

$$\frac{\partial \Psi}{\partial \zeta}\left[\frac{y_\eta \sin\gamma_2 + x_\eta \cos\gamma_2}{J}\right] - \frac{\partial \Psi}{\partial \eta}\left[\frac{y_\zeta \sin\gamma_2 + x_\zeta \cos\gamma_2}{J}\right] + B\Psi = 0. \tag{36}$$

5. Examples

5.1. Numerical simulations of wave propagation on a constant slope

The analytical–numerical solution of linear wave for refraction on a constant slope in the absence of current is given by Hong (1996)

$$\frac{H}{H_0} = K_s K_r K_f \tag{37}$$

where

$$K_s = \left(\frac{(c_g)_0}{c_g}\right)^{\frac{1}{2}} \tag{38}$$

$$K_r = \left(\frac{\cos\theta_0}{\cos\theta}\right)^{\frac{1}{2}} \tag{39}$$

$$\theta = \sin^{-1}\left(\frac{k_0}{k}\sin\theta_0\right) \tag{40}$$

$$K_f = \left\{1 + \frac{2H_0\omega^3}{3\pi g (c_g)_0 \cos\theta_0}\int_{x_0}^{x} f_w \left(\frac{K_r K_s}{\sinh(kh)}\right)^3 \mathrm{d}x\right\}^{-1} \tag{41}$$

$(c_g)_0$ and k_0 respect wave group velocity and wave number respectively at the initial boundary.

5.1.1. The adaptability of the present model to oblique incidence

When the bottom has a constant slope with a certain gradient, the wave propagation problem is reduced to a pure refraction one. The incident wave period and height are chosen as 6.21 s and 3.0 m respectively. The water depth is chosen as 40.0 m at the initial boundary, and the slope of bottom is set as 1:10. The incident wave angle is chosen as 60°. The space step and time step are chosen as 8.0 m and 3.0 s respectively. The calculation results are shown in Fig. 2. Fig. 2 shows that the results of numerical model are in agreement with those of analytical model in the case of oblique incidence.

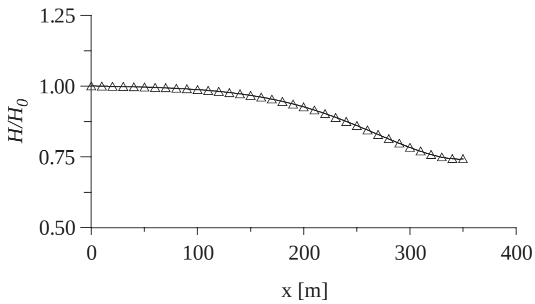

Fig. 2. Comparison of wave heights between numerical solution and analytical solution on a constant slope of 1:10. (—) Numerical solution; (△) analytical solution.

5.1.2. The effects of dissipation term on wave propagation

The water depth is constant and chosen as 10.0 m. The incident wave period and height are also chosen as 6.21 s and 3.0 m respectively. The wave is normal incidence. The influence of different dissipation coefficients $f_w = 0.005$ and $f_w = 0.01$ on calculation results is shown in Fig. 3. The calculation results show that the influence of dissipation term on calculation results becomes bigger and bigger with the distance of wave propagation increasing. Fig. 3 shows that the effects of dissipation term should be taken into account if the distance of wave propagation is larger than 2 km or so.

5.2. Waves between symmetric diverging breakwaters

For the waves between diverging breakwaters which satisfies no-flow boundary conditions is shown in Fig. 4, KDK introduced the exact solution based on the original mild slope equation and the analytic solution of small angle parabolic approximation.

For stationary monochromatic wave with frequency ω and without dissipation term, Eq. (1) is reduced to a variable-coefficient Helmholtz one (Radder, 1979; KDK).

$$\Phi_{xx} + \Phi_{yy} + K'^2\Phi = 0 \tag{42}$$

where

$$\phi(x,y,t) = \sqrt{cc_g}\Phi(x,y)e^{-i\omega t} \tag{43}$$

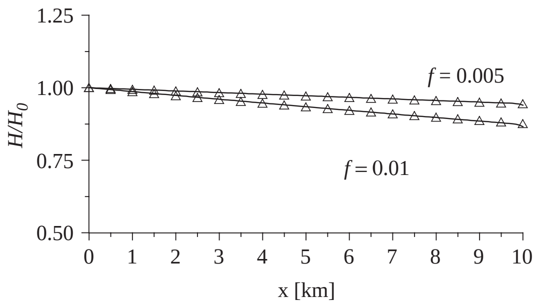

Fig. 3. Comparison of wave heights between numerical solution and analytical solution in waters of constant depth ($h = 10$ m) considering dispersion term. (——)Numerical solution; (△) analytical solution.

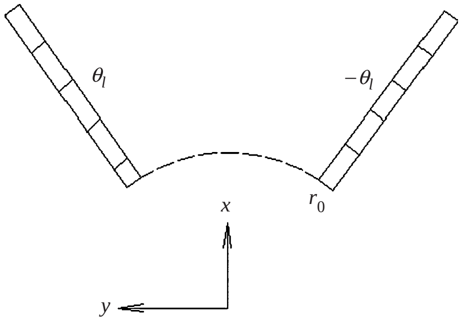

Fig. 4. General configuration of diverging breakwaters.

$$K'^2 = k^2 - \frac{\left(\sqrt{cc_g}\right)_{xx} + \left(\sqrt{cc_g}\right)_{yy}}{\sqrt{cc_g}} \tag{44}$$

For the case of constant depth, $K' = k$.

$$\omega^2 = gk\tanh(kh) \tag{45}$$

in which $c = ((\omega)/(k))$ and $c = ((\partial\omega)/(\partial k))$.

5.2.1. The exact solution based on the original mild slope equation

In a polar coordinate, Eq. (42) is transformed into

$$\Phi_{rr} + \frac{1}{r}\Phi_r + \frac{1}{r^2}\Phi_{\theta\theta} + k^2 = 0 \tag{46}$$

KDK obtained the exact solution for Eq. (46) that satisfies no-flow boundary condition at $\theta = \pm\theta_\ell$ as follows:

$$\Phi(r,\theta) = \sum_{n=0}^{\infty} a_n H_{\beta_n}^{(1)}(kr)\cos[\beta_n(\theta + \theta_\ell)] \tag{47}$$

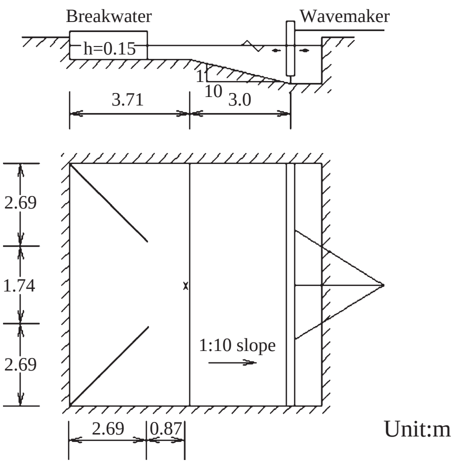

Fig. 5. Experimental configuration.

The incident plane wave at the breakwater entrance $r=r_0$ is

$$\eta_I = \frac{a}{2}\mathrm{e}^{ikr_0\cos(\theta-\theta_0)} + \mathrm{c.c.} = A(r_0,\theta)\mathrm{e}^{ikr_0} + \mathrm{c.c.} \tag{48}$$

where

$$A(r_0,\theta) = \frac{a}{2}\mathrm{e}^{-ikr_0}\left\{J_0(kr_0) + \sum_{m=1}^{\infty} 2(i)^m J_m(kr_0)\cos[m(\theta-\theta_0)]\right\} \tag{49}$$

Here, we correct the error of Eq. (B6) in Appendix B of KDK.

Assuming $\Phi(r_0,\theta)=G(\theta)$, where $G(\theta)=A(r_0,\theta)\mathrm{e}^{ikr_0}$ and using the orthogonality of the cosines over the range $-\theta_l \le \vartheta \le \theta_l$, KDK obtained

$$a_n = \frac{\varepsilon_n \int_{-\theta_\ell}^{\theta_\ell} G(\theta)\cos[\beta_n(\theta+\theta_\ell)]\mathrm{d}\theta}{2\theta_\ell H_{\beta_n}^{(1)}(kr_0)} \quad n=0,1,2,3,..... \tag{50}$$

$\varepsilon_n=1$ for $n=0$, and $\varepsilon_n=2$ otherwise.

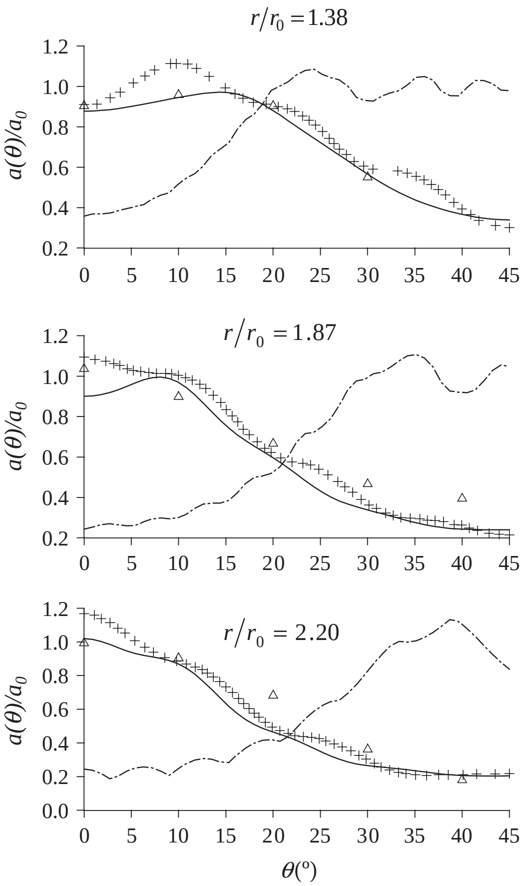

Fig. 6. Comparison of the results of relative amplitudes along constant r lines. (——) Exact solution of this paper; (+) exact solution of KDK; (– - - – –) analytical solution of small-angle parabolic approximation of KDK; (△) experimental data.

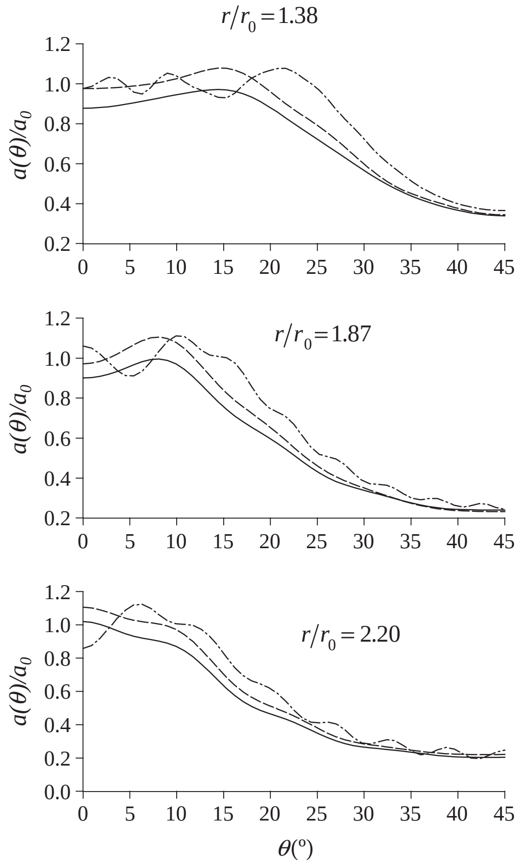

Fig. 7. Comparison of the results of relative amplitudes along constant r lines. (——) Exact solution of this paper; (– – –) solution of the present numerical model; (– - - - –) analytical solution of small-angle parabolic approximation of this paper.

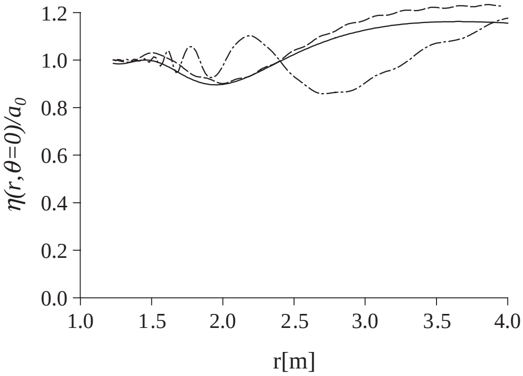

Fig. 8. Comparison of the results of relative amplitudes along centerline $\theta = 0$. (——) Exact solution; (– – –) solution of the present numerical model; (– - - - –) analytical solution of small-angle parabolic approximation of this paper.

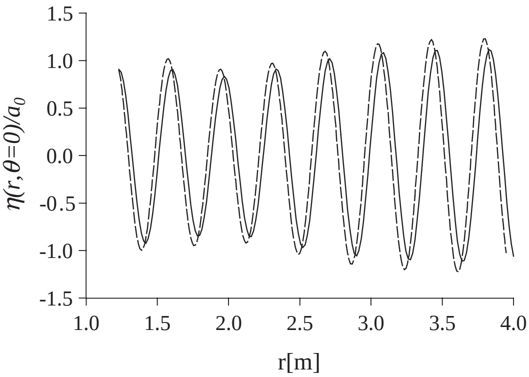

Fig. 9. Comparison of relative surface displacement $\eta(r)/a_0$ along centerline $\theta = 0$. (——) Exact solution; (– – –) solution of the present numerical model.

5.2.2. The approximation solution of small angle parabolic model

Having r as the preferred propagation direction and assuming $\Phi(r,\theta) = Re\left(A(r,\theta)\mathrm{e}^{i\int KJ^{\frac{1}{2}}\mathrm{d}r}\right)$, from Eq. (42) KDK introduced the small angle parabolic equation

$$2ikr^2A_r + ikrA + A_{\theta\theta} = 0. \tag{51}$$

For the waves between symmetric diverging breakwaters shown in Fig. 4, KDK obtained the solution of Eq. (51). The expressions of the above solution are expressed by (B3) and (B7)–(B9) in Appendix B of KDK. But we find that the solution expressions of KDK are wrong. The correct expressions should be written as

$$A(r,\theta) = \left[a_0 + \sum_{n=1}^{\infty} a_n \mathrm{e}^{i\left(\frac{n^2\pi^2}{8\vartheta_\ell^2 kr}\right)} \cos[\beta_n(\theta + \theta_\ell)]\right] r^{-\frac{1}{2}}, \tag{52}$$

where

$$a_0 = ar_0^{\frac{1}{2}}\mathrm{e}^{-ikr_0}\left\{J_0(kr_0) + \sum_{m=1}^{\infty}\frac{2(i)^m}{m\theta_\ell}J_m(kr_0)\sin(m\theta_\ell)\cos(m\theta_0)\right\}, \tag{53}$$

$$a_n = 2ar_0^{\frac{1}{2}}\mathrm{e}^{-i\left[kr_0 + \frac{n^2\pi^2}{8kr_0\vartheta_\ell^2}\right]}\sum_{m=1}^{\infty}(i)^m J_m(kr_0)I_{m,n}^1, \tag{54}$$

$$I_{m,n}^1 = \begin{cases} \left(\dfrac{1}{2m\vartheta_\ell + n\pi} + \dfrac{1}{2m\vartheta_\ell - n\pi}\right)\{[(-1)^n + 1]\sin(m\theta_\ell)\cos(m\theta_0) + [-(-1)^n + 1]\cos(m\theta_\ell)\sin(m\theta_0)\}, & m \neq \frac{n\pi}{2\theta_\ell} \\ \cos(m\theta_0 + \dfrac{n\pi}{2}), & m = \frac{n\pi}{2\theta_\ell} \end{cases} \tag{55}$$

in which J_m is the Bessel function of first kind and order m.

Table 1
The calculated index d with the relative amplitude of exact solution as $x(j)$

$y(j)$	Section			
	$r/r_0 = 1.38$	$r/r_0 = 1.87$	$r/r_0 = 2.20$	$\theta = 0°$
Relative amplitude of the present numerical solution	0.981	0.990	0.991	0.965
Relative amplitude of analytical solution of this paper	0.931	0.960	0.964	0.425

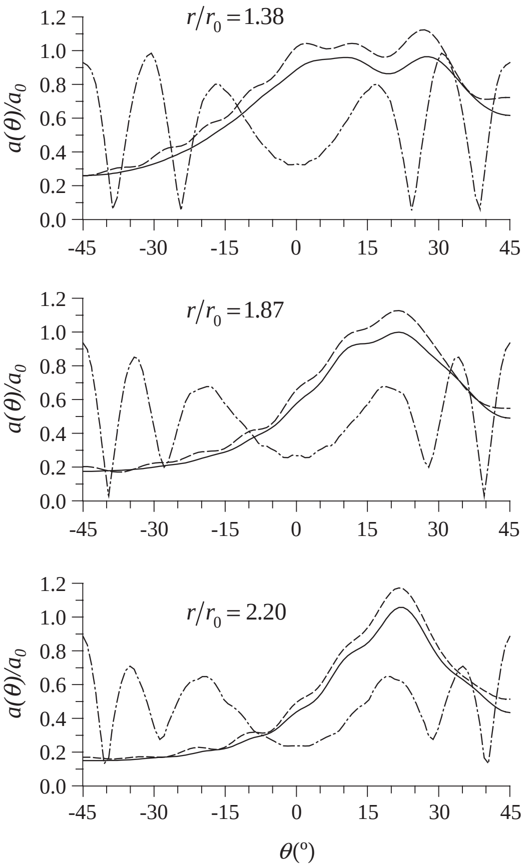

Fig. 10. Comparison of the results of relative wave amplitudes along constant r lines for the incident angle being 30°. (——) Exact solution; (– – –) numerical solution; (– - - - –) analytical solution of small-angle parabolic approximation of KDK.

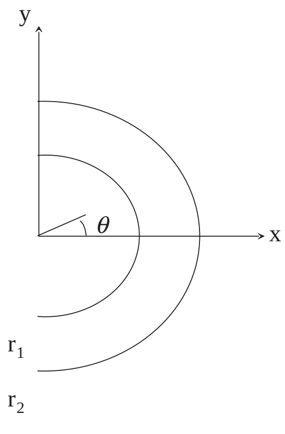

Fig. 11. Configuration of circular channel.

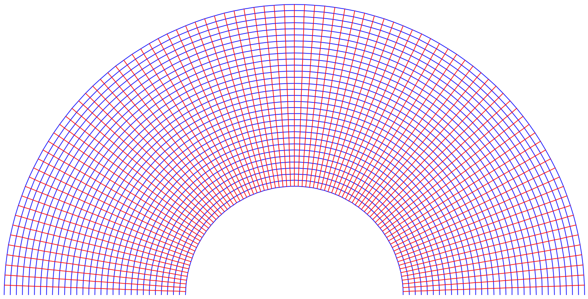

Fig. 12. Calculation grid in the circular channel.

If the r-axis is placed along one breakwater, the angle of the other breakwater is $\theta_{\ell}=90^{\circ}$. The solution of small angle parabolic model can be expressed as another set of expressions, and the details can be seen in Appendix B.

5.2.3. Comparison of the results of different mathematical models

To test the application of the conformal mapping technique to the symmetric diverging breakwaters, Kaku and Kirby (1988) performed a series of experiments. The geometry of the breakwaters and the water depth are shown in Fig. 5. The breakwater enclosed a 90° sector with a gap of 1.74 m width. The water depth at the wavemaker is 0.45 m and decreased with a slope 1:10 up to the horizontal part. The incident wave is normal to the gap of breakwaters. The wave period T and amplitude a_0 are 0.49 s and 0.017 m respectively. The details of the experiment can be seen in the paper of KDK.

In order to compare to the results shown in Fig. 4 of KDK, the calculation domain is limited to the range 1.23 m$\leq r \leq$4.0 m in this paper. For the calculation of the exact solution and the analytical solution of small angle parabolic model, 177 and 100 steps are taken along the r and θ direction respectively. Fig. 6 shows that the correct results can not be obtained from the analytic solution of small angle approximation given by KDK and that the curves of the exact results of KDK obtained based on the original mild-slope equation are not sufficiently smooth. We verify that Order 25 should be remained calculating the cylindrical functions of relevant equations, otherwise the calculated curves will deviate from the true values. For the calculation of the numerical results, 265 and 100 steps are taken along the r and θ direction respectively, and Δt is taken as 0.07 s. In the process of numerical calculation, we find that the amount of bottom dissipation coefficient near the outgoing boundary basically does not influence the calculation results. We think that the reason should be the incident wave being normal and the wave direction at the open boundary varying not much. The results of relative wave amplitude of different models along three lines of constant distance r from the coordinate origin are shown in Fig. 7. Figs. 8 and 9 represent the comparison of the results of relative wave height and surface displacement along the centerline $\theta=0$ respectively.

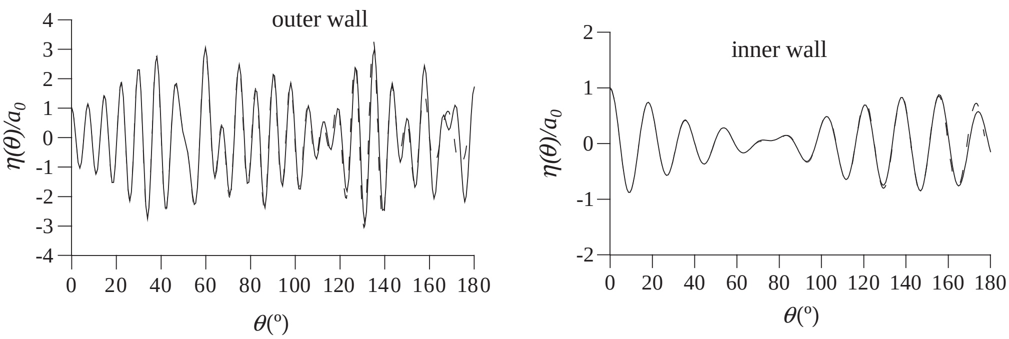

Fig. 13. Comparison of relative surface variation along inner and outer wall. (——) Numerical solution; (– – –) exact solution.

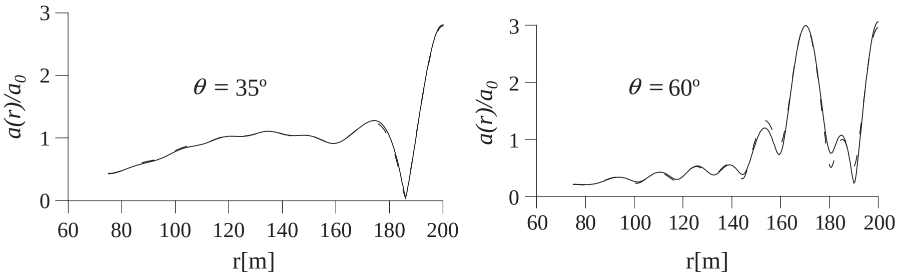

Fig. 14. Comparison of relative wave amplitudes on sections. (——) Numerical solution; (– – –) exact solution.

The quantitative mismatch can be measured by the index proposed by Wilmott (1981) as follows:

$$d = 1 - \frac{\sum_{j=1}^{n} [y(j) - x(j)]^2}{\sum_{j=1}^{n} [|y(j) - \bar{x}| + |x(j) - \bar{x}|]^2} \tag{56}$$

where $x(j)$ are the true values, $\bar{x}$ is the mean value of $x(j)$, and $y(j)$ are the calculation results. $d=0$ means a completely mismatch and $d=1$ indicates a perfect agreement (Shi et al., 2001).

Figs. 7–9 and Table 1 show that the results of the present numerical model are in agreement with those of the exact solution and apparently outperform those of the analytic solution based on the small angle parabolic model. Fig. 8 shows that the longer distance the waves propagate the bigger errors the small-angle parabolic model generates. For this example, KDK pointed out that the large angle parabolic model only partially improved the calculation results. So the present numerical model provides better results than the parabolic models for this example.

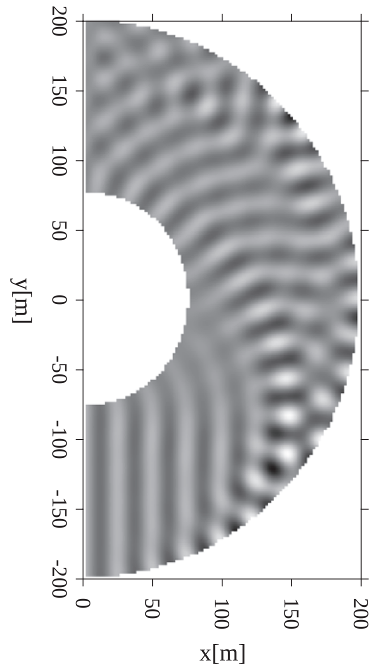

Fig. 15. Relative wave surface of numerical simulation.

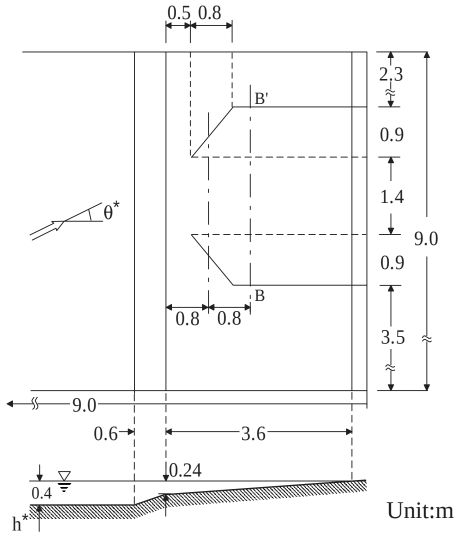

Fig. 16. Laboratory setup.

To further verify the adaptability of the present numerical model and show the mistakes of the analytical solution of small angle approximation given by KDK, the results of oblique incident angle $\theta_0=((\pi)/(6))$ are shown in Fig. 10. The calculation results show that the analytical solution of small angle approximation given by KDK is obviously wrong. By the way, it is only a stray coincidence that contraposition of the curves plotted with the analytical solution of small angle approximation given by KDK is in agreement with the correct curves in the case of normal incidence.

5.3. Waves in circular channel

Based on the mild slope equation in a polar coordinate, KDK obtained the exact solution of waves in a circular channel shown in Fig. 11. The channel lies between two radii, $r_1=75$ m and $r_2=200$ m, and covers a 180° arc. The water depth and incident wave period are 10 m and 4.0 s respectively. Plane waves with a uniform amplitude enter at the bottom right of the figure and propagate around the bend in a counter-clockwise direction. For the calculation of the numerical solution, the time step is chosen as 1.0 s. A 250×250-grid mesh in the physical domain is shown in Fig. 12. The grid spacing in the radial direction is constant at 0.5 m, while a constant angular grid is used along the channel length. In this example, the bottom dissipation coefficient of four rows of grids near the open boundary is set large enough to dissipate the waves to small. Otherwise the correct results can not be

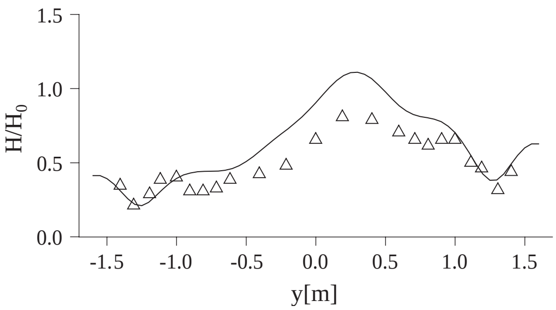

Fig. 17. Comparison of relative wave heights on transect B–B′. (—) Numerical solution; (△) experimental data.

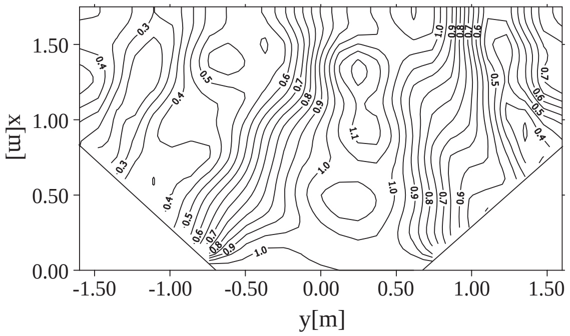

Fig. 18. Contour of numerical simulation wave heights.

obtained. The reason is that the wave directions near the open boundary vary severely and cannot be exactly calculated by iteration. The calculated results are shown in Figs. 13–15. The calculated index d with the relative amplitude of exact solution as $x(j)$ and numerical solution as $y(j)$ are 0.996 and 0.980 along the inner and outer wall respectively. KDK provided the numerical results of parabolic models. We calculated that the index d is 0.952 with the results of KDK based on the large angle parabolic model along the outer wall. For this case, the results of large angle parabolic model are in much stronger agreement with the exact solution than the small angle model (KDK). Shi et al. (2001) calculated that the index d are 0.984 and 0.991 with the results of Boussinesq-type model as $y(j)$ along the inner and outer wall respectively. For this example, the present numerical model provides better results than the parabolic models, and it has about the same precision as the Boussinesq-type model. However, the Boussinesq-type model requires much more computer time.

5.4. Oblique waves in breakwater harbor

Isobe (1986) performed an experiment for oblique wave in a breakwater harbor whose geometry and water depth are shown in Fig. 16. The incident wave angle, period and height are 18°, 0.83 s and 0.091 m respectively (Liu and Bolssevain, 1988; Kirby, 1988). The wave height along the initial line was assumed to be constant. Used

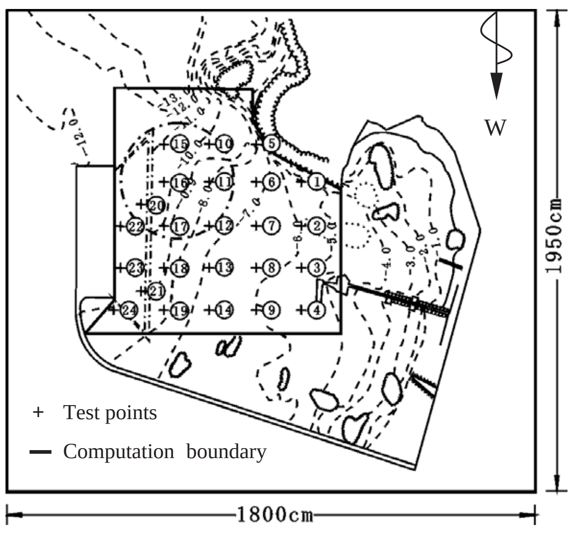

Fig. 19. Arrangement of test point and configuration of computation boundary.

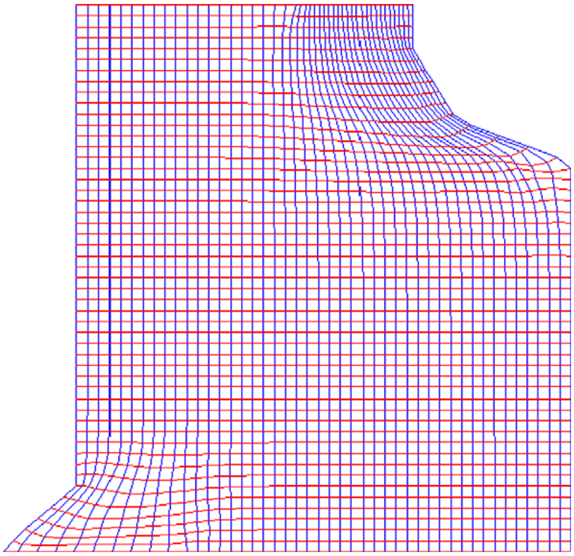

Fig. 20. Calculation grid in the computation domain.

Snell's law, the incident wave angle at the harbor mouth is calculated to be 16.03°. A 41 × 65-grid mesh is adopted in the physical domain. The numerical results are shown in Figs. 17 and 18. Fig. 17 shows that the numerical results are basically agreement with the experimental data. The difference between them could result from a number of factors (Kirby, 1988). Fig. 18 shows that the present numerical model is able to reflect the influences of boundary on the distribution of wave height under the condition of oblique waves.

5.5. Wave transformation in water region with complicated boundaries

The water front of a wharf is from east to west. The length of the water front is 400 m. The inlet of the port is in the east. The main objective of hydraulic model experiment is to determine the distribution of wave height under

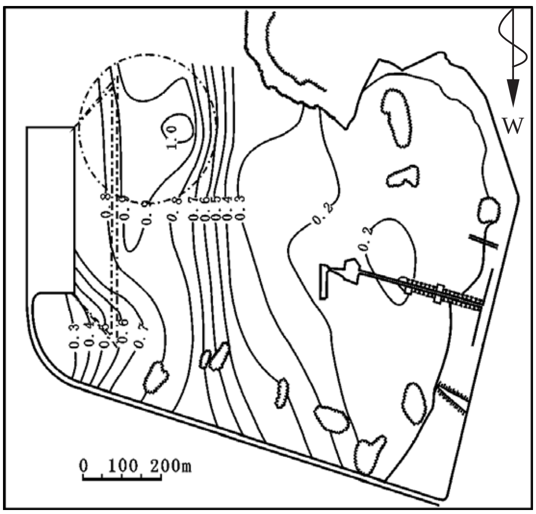

Fig. 21. Contour of relative wave heights from experiment.

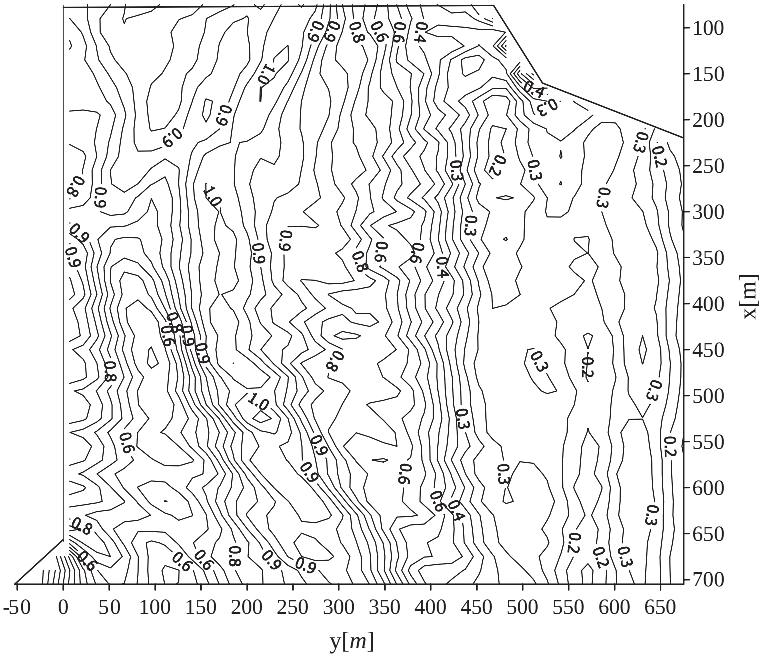

Fig. 22. Contour of relative wave heights from numerical simulation.

the condition of east incident wave (Zhang, 2000). The experimental arrangement is illustrated in Fig. 19. For simplicity, the area excluding the reefs is chosen as the computation domain. A 100×90-grid mesh in the computation domain is shown in Fig. 20.

The incident wave height and period are 5.02 m and 8.0 s respectively. The edge of the harbor is crooked and complicated, and the boundary of the wharf is a rigid vertical wall, thus the boundary condition is that the normal flux vanishes. The boundaries of the reefs are partially reflective, and the reflective coefficients are set as 0.4. The distributions of relative wave height from experiment and numerical solution are shown in Figs. 21 and 22 respectively. The detailed comparison of different results is shown in Table 2. Although the water depth is obtained through interpolation from topographic map and the computation domain is simplified, the numerical results basically correspond to experimental ones. Table 2 shows that the maximum, minimum and average error are 15.38%, 0% and 5.96% respectively. Fig. 22 shows that the wave heights in the wave shadow are very small. Generally, the present model can effectively reflect the effects of boundaries on wave distribution.

6. Conclusion

In curvilinear coordinates, a numerical model for wave propagation including dissipation term in water of slowly varying topography is presented employing self-adaptive methods. The effects of dissipation term should be taken into account if the distance of wave propagation is larger than 2 km or so. If the wave angles are small and vary not much near the open boundary, the amount of bottom dissipation coefficient basically does not influence the calculation results. If the wave angles vary severely near the open boundary, the bottom dissipation coefficient has to be set large enough to dissipate the waves to small, otherwise the correct results can not be obtained. In this paper, the waves propagation between diverging breakwaters is studied in detail. The order of the cylindrical function should be remained more than 25 calculating the relevant equations; the errors of the analytical solution that KDK deduced from the small-angle parabolic approximation of the mild-slope equation are corrected. The calculation of the waves

Table 2
Table of comparison between measured and computed relative wave heights

Point no.	H_p	H_m	$\lvert H_p - H_m \rvert$	$((\lvert H_p - H_m \rvert)/(H_p))$ (%)
1	0.30	0.280	0.020	6.67
2	0.28	0.300	0.020	7.14
3	0.19	0.193	0.003	1.55
4	0.26	0.220	0.040	15.38
5	0.34	0.371	0.031	8.82
6	0.31	0.291	0.019	6.45
7	0.26	0.264	0.004	1.64
8	0.33	0.335	0.005	1.52
9	0.38	0.398	0.018	4.69
10	0.87	0.810	0.060	6.90
11	1.05	0.910	0.140	13.33
12	0.81	0.765	0.045	5.59
13	0.77	0.77	0.000	0.00
14	0.92	0.960	0.040	4.31
15	0.91	0.950	0.040	4.40
16	1.03	1.02	0.011	1.11
17	1.02	1.016	0.004	0.40
18	0.90	0.801	0.091	11.10
19	0.65	0.620	0.030	4.62
20	0.79	0.743	0.047	6.00
21	0.70	0.715	0.015	2.21
22	0.78	0.880	0.100	12.82
23	0.74	0.820	0.080	10.81
24	0.33	0.349	0.019	5.68

H_p represents the measured wave heights and H_m represents computed relative wave heights.

in a circular channel shows that the results of the present model are in agreement with the exact solution. This numerical model effectively simulates the complex wave pattern resulting from the superposition of the incident wave, diffraction and re-reflection. For the above two cases, the present numerical model provides better results than the parabolic models. The detailed numerical tests show that the present numerical model is able to adapt to complicatedly boundaries and varying depth.

For practical application in coastal engineering more effectively, the present model needs to be further improved with the external objects in the water region, especially the objects with varying reflection coefficients.

Acknowledgements

This study is supported by the National Natural Science Foundation of China (Grant No.: 40106008) and by LED, South China Sea Institute of Oceanology, Chinese Academy of Sciences.

Appendix A. A derivation of the mathematical model with dissipation term for combined refraction–diffraction waves in the current-free case

The problem of gravity surface wave for an irrotational ideal fluid is reduced for the velocity potential $\varphi(x,y,z,t)$, satisfying

$$\nabla^2\varphi + \varphi_{zz} = 0, \qquad \nabla = \left(\frac{\partial}{\partial x}, \frac{\partial}{\partial y}\right) \qquad -h \prec z \prec 0 \tag{A1}$$

$$g\varphi_z + \left(\frac{\partial}{\partial t} + W^*\right)\frac{\partial \varphi}{\partial t} = 0 \quad z = 0 \tag{A2}$$

where W^* is the energy dissipation term,

$$\varphi_z + \nabla\varphi \cdot \nabla h = 0 \quad z = -h. \tag{A3}$$

The linear solution is defined as:

$$\varphi(x,y,z,t) = f(h,z,x,y)\phi(x,y,t) \tag{A4}$$

and

$$\phi = -igR(x,y,t)e^{i\psi(x,y,t)} = Re\phi + Im\phi$$
$$= \phi_1 + i\phi_2 \tag{A5}$$

According to (A5), we can obtain the following relations:

$$\omega = -\frac{\partial \psi}{\partial t} = -\frac{\left(\phi_1 \frac{\partial \phi_2}{\partial t} - \phi_2 \frac{\partial \phi_1}{\partial t}\right)}{|\phi|^2}. \tag{A6}$$

For simplicity, the following non-dimensional parameters are introduced:

$$\varepsilon = ka, \qquad \delta = \frac{\nabla h}{kh}, \qquad \beta = \frac{\frac{\partial w}{\partial t}}{\omega^2}, \qquad \gamma = \frac{\frac{\partial R}{\partial t}}{\omega R}$$

Substituting Eqs. (A4) and (A5) into the boundary condition (A2) yields

$$gf_z - f\sigma^2\left\{1+\frac{1}{4}\left(\beta^2+\frac{W*^2}{\omega^2}\right)+\frac{1}{2\omega}\frac{\partial\beta}{\partial t}\right\}=0,$$
$$z=0 \tag{A7}$$

and its solution is

$$f(h,z)=\frac{\cosh[k(z+h)]}{\cosh(kh)} \tag{A8}$$

and

$$\omega^2\left(1+\frac{1}{4}\beta^2+\frac{1}{2\sigma}\frac{\partial\beta}{\partial t}\right)=\tilde{\sigma}^2-\frac{1}{4}W*^2 \tag{A9}$$

or

$$\omega^2=\tilde{\sigma}^2-\frac{1}{4}W*^2, \qquad \beta \prec\ \prec 1 \tag{A9$'$}$$

$$\tilde{\sigma}^2=gk\tanh(kh) \qquad \tilde{\sigma}=k\tilde{c}, \qquad \tilde{c}_g=\frac{\partial\tilde{c}}{\partial k} \tag{A10}$$

Substituting (A4) into (A3) gives:

$$(\nabla(kh)\nabla h)\tanh(kh)+(\nabla h\nabla\phi)/\phi=O(\delta^2)=0,$$
$$z=-h(x,y) \tag{A11}$$

In order to find the unknown function ϕ, we integrate vertically the Eq. (1) with the weighted function of $f(h,z)$, that is

$$\int_{-h}^{0} f\left(\nabla^2\phi+\phi_{zz}\right)\mathrm{d}z=0 \tag{A12}$$

By means of transformations and neglecting the high order terms of ε, δ and β, we obtain:

$$\frac{\partial}{\partial t}\left(\frac{\partial}{\partial t}+W*\right)\phi-\nabla\left(\tilde{c}\tilde{c}_g\nabla\phi\right)+\left(\tilde{\sigma}^2-k^2\tilde{c}\tilde{c}_g\right)\phi=0 \tag{A13}$$

Appendix B. Another form of the analytic solution for the small-angle parabolic model for symmetrical breakwaters in polar coordinates: the r axis is placed along one breakwater

If the r-axis is placed along one breakwater, the angle of the other breakwater is $\theta_\ell=90°$. The normal incidence hence becomes $\theta_0=45°$. The equation corresponding to Eq. (B3) of KDK should be expressed as

$$A(r,\theta)=\left[a_0+\sum_{n=1}^{\infty}a_n \mathrm{e}^{i\left(\frac{n^2\pi^2}{2kr\theta_\ell^2}\right)}\cos(\beta_n\theta)\right]r^{-\frac{1}{2}} \tag{B1}$$

where

$$\beta_n=\frac{n\pi}{\theta_\ell} \tag{B2}$$

The equation corresponding to Eq. (B7) of KDK should be expressed as

$$a_0=ar_0^{\frac{1}{2}}\mathrm{e}^{-ikr_0}\left(J_0(kr_0)+\sum_{m=1}^{\infty}\frac{2(i)^m}{m\theta_\ell}J_m(kr_0)\right.$$
$$\left.\times\left\{\sin[m(\theta_\ell-\theta_0)]+\sin(m\theta_0)\right\}\right) \tag{B3}$$

The equation corresponding to Eq. (B8) of KDK should be expressed as

$$a_n=2ar_0^{\frac{1}{2}}\mathrm{e}^{-i\left[kr_0+\frac{n^2\pi^2}{2kr_0\theta_\ell^2}\right]}\sum_{m=1}^{\infty}(i)^m J_m(kr_0)I^1_{m,n} \tag{B4}$$

where

$$I^1_{m,n}=\begin{cases}\left(\frac{1}{m\theta_\ell+n\pi}+\frac{1}{m\theta_\ell-n\pi}\right)\left\{(-1)^n\sin(m\theta_\ell-m\theta_0)+\sin(m\theta_0)\right\}, & m\neq\frac{n\pi}{\theta_\ell}\\ \cos(m\theta_0) & m=\frac{n\pi}{\theta_\ell}\end{cases} \tag{B5}$$

The results obtained from above equations are the same as those from Eqs. (52)–(55).

References

Berkhoff, J.C.W., 1972. Computation of combined refraction–diffraction. Proc. 13th Conference on Coastal Engineering, vol. 1. ASCE, Vancouver, Canada, pp. 471–490.

Berkhoff, J.C.W., Booij, N., Radder, A.C., 1982. Verification of numerical wave propagation models for simple harmonic linear water waves. Coastal Engineering 6, 255–279.

Brackbill, J.U., Saltzman, J.S., 1982. Adaptive zoning for singular problems in two dimensions. Journal of Computational Physics 46, 342–368.

Copeland, G.J.M., 1985. A practical alternative to the mild-slope wave equation. Coastal Engineering 9, 125–149.

Hong, G.W., 1996. Mathematical models for combined refraction–diffraction of waves on non-uniform current and depth. China Ocean Engineering 10 (4), 433–454.

Hong, G.W., Zhang, H.S., Feng, W.B., 1998. Numerical simulation of nonlinear three-dimensional waves in water of arbitrary varying topography. China Ocean Engineering 12 (4), 383–404.

Hong, G.W., Feng, W.B., Zhang, H.S., 1999. Numerical modeling of wave propagation in water of varying topography and current. Journal of Hohai University 27 (2), 1–9 (in Chinese).

Isobe, M., 1986. A parabolic refraction–diffraction equation in the ray-front coordinate system. Proceedings 20th International Coastal Engineering Conference, Taipei, pp. 306–317.

Kaku, H., Kirby, J.T., 1988. A parabolic equation method in polar coordinates for waves in harbors. Tech. Report UFL/COEL-TR/075, Coastal and Oceanographic Engineering Department, University of Florida, Gainesville, FL.

Kirby, J.T., 1988. Parabolic wave computations in non-orthogonal coordinate systems. Journal of Waterway, Port, Coastal, and Ocean 114 (6), 673–685.

Kirby, J.T., Dalrymple, R.A., Kabu, H., 1994. Parabolic approximation for water waves in conformal coordinate systems. Coastal Engineering 23, 185–213.

Li, B., 1994. An evolution equation for water waves. Coastal Engineering 23, 227–242.

Li, B., Anastasiou, K., 1992. Efficient elliptic solvers for the mild-slope equation using the multigrid technique. Coastal Engineering 16, 245–266.

Liu, P.L.F., Bolssevain, P.L., 1988. Wave propagation between two breakwaters. Journal of Waterway, Port, Coastal, and Ocean Engineering 114 (2), 237–247.

Liu, Z., Zeng, Q., 1994. The preliminary application of adaptive mesh in the problems of atmosphere and ocean. Scientia Atmospherica Sinica 18 (6), 641–648 (in Chinese).

Pan, J.N., Zuo, Q.H., Wang, H.C., 2000. Efficient numerical solution of the modified mild-slope equation. China Ocean Engineering 14 (2), 161–174.

Panchang, V.G., Cushman-Roisin, B., Pearce, B.R., 1988. Combined refraction–diffraction of short-waves in large coastal regions. Coastal Engineering 12, 133–156.

Panchang, V.G., Pearce, B.R., Wei, G., Cushman-Roisin, B., 1991. Solution of the mild-slope wave problem by iteration. Applied Ocean Research 13 (4), 187–199.

Radder, A.C., 1979. On the parabolic equation method for water-wave propagation. Journal of Fluid Mechanics 95, 159–176.

Shi, F.Y., Sun, W.X., 1995. A variable boundary model of storm surge flooding in generalized curvilinear coordinate grids. International Journal for Numerical Methods in Fluids 21, 641–651.

Shi, F.Y., Sun, W.X., Wei, G.S., 1997. A WDM method on a generalized curvilinear grid for calculation of storm surge flooding. Applied Ocean Research 19, 275–282.

Shi, F.Y., Dalrymple, R.A., Kirby, J.T., Chen, Q., Kennedy, A., 2001. A fully nonlinear Boussinesq model in generalized curvilinear coordinates. Coastal Engineering 42, 337–358.

Smith, R., Sprinks, T., 1975. Scattering of surface waves by a conical island. Journal of Fluid Mechanics 72, 373–385.

Wilmott, C.J., 1981. On the validation of models. Physical Geography 2, 219–232.

Zhang, H.S., 2000. Numerical simulation of non-linear wave propagation. PhD dissertation, Nanjing: Hohai University, 39–44 (in Chinese).

Zhang, H.S., 2002. Mathematical Models of Wave Propagation in Coastal Region. East China Normal University, Shanghai (in Chinese).

Zhang, H.S., Ding, P.X., Pan, J.N., Hong, G.W., 2003. Numerical simulation of a mathematical model for wave propagation on non-uniform current and depth. Journal of Hydrodynamics. Series B 2, 43–50.